The relationship between the Guinea Highlands and the West African offshore rainfall maximum

H. L. Hamilton[1] (iD), G. S. Young[1] (iD), J. L. Evans[1] (iD), J. D. Fuentes[1] (iD), and K. M. Núñez Ocasio[1,2] (iD)

[1]Department of Meteorology and Atmospheric Science, Pennsylvania State University, University Park, Pennsylvania, USA, [2]Department of Physics, University of Puerto Rico at Mayagüez, Mayagüez, Puerto Rico

Abstract Satellite rainfall estimates reveal a consistent rainfall maximum off the West African coast during the monsoon season. An analysis of 16 years of rainfall in the monsoon season is conducted to explore the drivers of such copious amounts of rainfall. Composites of daily rainfall and midlevel meridional winds centered on the days with maximum rainfall show that the day with the heaviest rainfall follows the strongest midlevel northerlies but coincides with peak low-level moisture convergence. Rain type composites show that convective rain dominates the study region. The dominant contribution to the offshore rainfall maximum is convective development driven by the enhancement of upslope winds near the Guinea Highlands. The enhancement in the upslope flow is closely related to African easterly waves propagating off the continent that generate low-level cyclonic vorticity and convergence. Numerical simulations reproduce the observed rainfall maximum and indicate that it weakens if the African topography is reduced.

1. Introduction

A distinct maximum in accumulated rainfall occurs near the southwest coast of West Africa, where the strong large-scale convergence with the Intertropical Convergence Zone (ITCZ) interacts with the West African Monsoon (WAM) and topographic features. Near the West African coast is also where African easterly waves (AEWs) and their associated mesoscale convective systems (MCSs) attain maximum intensity [*Kiladis et al.*, 2006]. In a region where there are numerous driving factors in rainfall production, our objective is to understand why such a persistent rainfall maximum is located in a small area just offshore of West Africa.

Previous studies indicated distinct differences in the dynamic and thermodynamic characteristics of MCSs that propagate through West Africa and, in some cases, over the Atlantic Ocean [*DeLonge et al.*, 2010; *Jenkins et al.*, 2010; *Guy et al.*, 2011]. Previous studies employed satellite and radar data to examine convection and rainfall in West Africa [*Fuentes et al.*, 2008; *Nicholls and Mohr*, 2010; *Guy and Rutledge*, 2012]. These analyses showed that MCSs preferentially form at, and ahead of, the trough of AEWs in the southern part of the Sahel [e.g., *Mathon et al.*, 2002]. Previous studies show that the region of highest rainfall offshore the Guinea coast is dominated by deep convective storms and MCSs during the monsoon rainfall season [*Laing and Fritsch*, 1993; *Zipser*, 1994; *Xu and Zipser*, 2012].

Thorncroft and Hodges [2001] suggested that AEWs experience enhanced development over the Guinea Highlands, in association with orographic processes and latent heat release in deep moist convection. Also, *Thorncroft and Hodges* [2001] found that the growth region of AEWs to the west of the Guinea Highlands is collocated with the climatological rainfall maximum. A similar rainfall maximum occurs west of Mexico's Sierra Madre Mountains where another notable peak in AEW growth occurs [e.g., *Zehnder*, 1991; *Zehnder et al.*, 1999; *Thorncroft and Hodges*, 2001], creating a favored location for East Pacific tropical cyclogenesis [*Zehnder*, 1991; *Zehnder and Gall*, 1991; *Mozer and Zehnder*, 1996a, 1996b; *Zehnder et al.*, 1999]. The combined interaction of the ITCZ, easterly waves, and topography results in the cyclonic vorticity maxima of the waves to increase by 100% in the lee of the topography (with respect to the motion of the waves) [*Zehnder et al.*, 1999]. A similar interplay of topographic forcing, monsoon environment may explain the location of the climatological rainfall maximum in West Africa.

The maximum in rainfall is likely influenced by the elevated terrain in the West African region and further enhanced by the land-sea contrasts. In this study, we examine the offshore rainfall maximum in West Africa using Tropical Rainfall Measuring Mission (TRMM) satellite data and the European Centre for Medium-Range Weather Forecasts Re-Analyses (ERA)-Interim to create a 16 year climatology of rainfall. We

also employ the Weather Research and Forecast (WRF) model to perform simulations examining the sensitivity of the offshore rainfall maximum to upstream topography.

2. Data

Observations during May to October for 1998–2013 are used to examine rainfall variations in the WAM season and active periods of AEWs. This period spans the lifetime of the TRMM satellite [*Huffman et al.*, 2007].

We analyze the final gridded precipitation rates (p (mm hr^{-1})) from the version 7 TRMM Multi-satellite Precipitation Analysis 3-hourly product, 3B42 [*Huffman et al.*, 2007]. Daily precipitation measuring less than 0.2 mm (referred to as a trace) is ignored in this study based on the World Meteorological Organization definition [*World Meteorological Organization*, 2014]. We also utilize the rainfall data from the version 7 TRMM Precipitation Radar (PR) Level 2 Rainfall Rate and Profile Product, 2A25, which estimates the instantaneous three-dimensional distribution of rainfall from the TRMM precipitation radar data [*Kummerow et al.*, 1998].

Pressure level and surface meteorological data from ERA-Interim 6-hourly global atmospheric reanalysis were utilized in this study [*Dee et al.*, 2011]. We use variables such as zonal wind (u), meridional wind (v), vertical velocity (ω), specific humidity (q), and temperature (T) and derived quantities such as equivalent potential temperature (θ_e) and moisture divergence to analyze the atmospheric conditions influencing rainfall in the study region. The ERA-Interim data are also used as initial and boundary conditions in the WRF simulations described below.

## 3. Model Configuration and Design of Sensitivity Runs

To examine how topography influences the related initiation and development of MCSs over West Africa and the adjacent ocean, the WRF model version 3.7.1 with WRF Preprocessing System (WPS) version 3.7.1 [*Skamarock et al.*, 2008] is used to simulate three scenarios: realistic topography (hereafter called TOPO), topographic height smoothly reduced by 50% (HALF), and no topography (FLAT). Three one-way nested domains are employed with grid spacing of 36, 12, and 4 km (see Figure S1 in the supporting information). Each domain has 42 vertical levels extending from the surface to 50 hPa, distributed to provide the highest resolution in the lowest 1.5 km of the atmosphere (about 19 vertical levels). The parameterization schemes used are listed in Table S1 of the supporting information. We altered the African topography in all three domains; the terrain modification begins at sea level (e.g., Suez and Gibraltar) so that no terrain slope artifacts are introduced. Domain 1 encompasses regions outside Africa, but only the African topography was altered.

The WRF model is initialized at 0000 UTC 25 August 2006 and run for 36 days of simulation time for each of the three different scenarios. We modeled this specific period in order to compare results with observations made during the National Aeronautics and Space Administration African Monsoon Multidisciplinary Analyses. The statistics and analyses of these simulations described here are calculated on the second domain and exclude the first 12 h of each simulation to allow for model convection spin-up.

4. Rainfall Climatology

The 3-hourly TRMM 3B42 rainfall estimates are averaged over May to October to study the rainfall activity during the six West African Monsoon (WAM) months. During the WAM most of the rainfall occurs north of the equator with maxima in rainfall accumulation occurring over the Atlantic Ocean (Figures 1a–1f). The seasonal precipitation amount averaged over the 16 years displays the area of high rainfall accumulation over the Atlantic Ocean. These high accumulations are linked to the ITCZ where WAM southwesterlies converge with the northeasterly trade winds (Figure 1a). Annual rainfall accumulations of 2250–2750 mm occur within this zone just off the coast (Figure 1a). To examine why this small area experiences such copious amount of rainfall, we designate a study region spanning (20°–10°W, 5°–12°N), encompassing the offshore maximum in the averaged seasonal rainfall (Figure 1a). The area-averaged TRMM rainfall accumulation in the study region during the period 25 August to 30 September (captured in the WRF simulation) is 402.7 mm, 22% of its mean seasonal rainfall (1838.7 mm) (Figure 1b).

Comparison of the WRF spatial rainfall distribution over 25 August to 30 September 2006 from TOPO with that observed by TRMM indicates that the model captures the offshore rainfall maximum but produces substantially more rainfall in the region (1511 mm; Figure 1d) than observed (826 mm; Figure 1c).
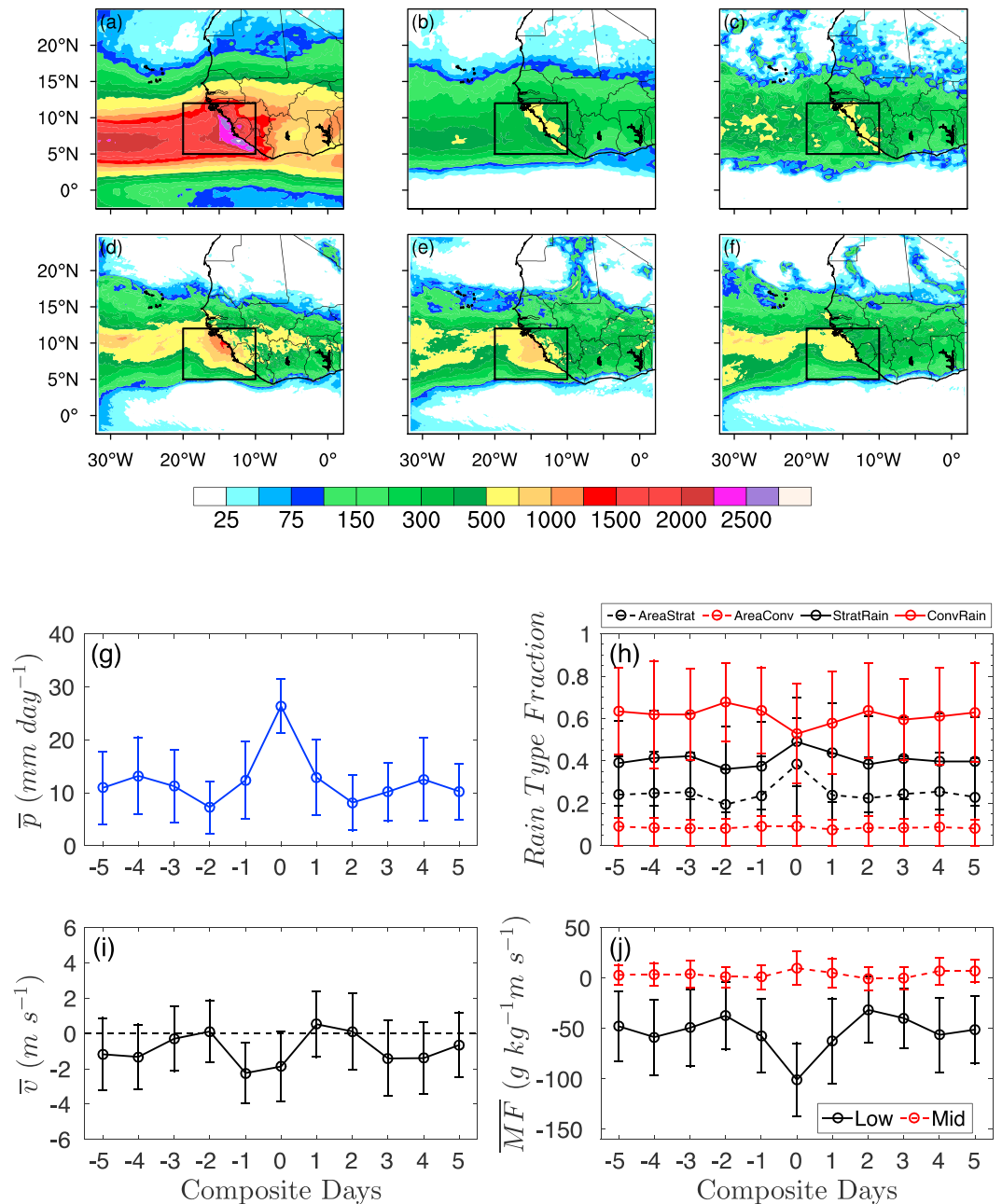
Figure 1. Average TRMM rainfall (mm) (a) accumulated over the monsoon season (May to October) 1998–2013 and (b) accumulated over 1200 UTC 25 August to 0000 UTC 30 September 1998–2013. Rainfall accumulated over 1200 UTC 25 August to 0000 UTC 30 September 2006 from (c) TRMM, and domain 2 of (d) TOPO, (e) HALF, and (f) FLAT. The inner box represents the study region from 20°–10°W and 5°–12°N. Composites of area-averaged (g) daily precipitation (mm day^{-1}) from TRMM 3B42, (h) rain type fraction (solid line) and rain type area fraction (dashed line) black = stratiform; red = convective, (i) meridional wind speed (m s^{-1}), and (j) moisture flux (black = low level, 1000–850 hPa; red = midlevel, 700–500 hPa) (g kg^{-1} m s^{-1}) centered on the five rainiest days (day 0) in August-September of each year in the period 1998–2013. The vertical bars indicate the range of daily values for the individual years.

Overproduction of convective rainfall is a common effect in numerical models and has been attributed to overprediction of convective intensity and poor microphysics parameterization [e.g., *Varble et al.*, 2014a, 2014b]. The area-averaged total rainfall accumulation over the 35 days is 373.81 mm based on TRMM rainfall estimates and 597.99 mm in TOPO, which is about 32% of the observed mean seasonal total. The area-averaged total rainfall accumulation decreases as the height of topography is reduced—509.84 mm in

HALF and 390.67 mm in FLAT, with the offshore rainfall maximum weakening until it becomes indistinguishable from the general ITCZ convection (Figures 1d–1f). These results suggest that the climatological offshore rainfall maximum is linked to the upstream topography. The lack of forced topographic uplift when topography is removed will undoubtedly affect convective development near the coast. However, in *Hamilton* [2016], the progressive reduction of topography also led to the weakening of the (AEJ) and the reduced growth of AEWs as they propagated downstream. Since the Guinea Highlands have been identified as a region where AEWs may experience enhanced development [*Thorncroft and Hodges*, 2001], we hypothesize a connection between AEWs and the weakening of the offshore rainfall maximum. We next examine the atmospheric conditions that lead to the offshore rainfall maxima observed in the TRMM data and obtained with WRF simulations.

5. Rainfall Composites

We construct area-averaged TRMM daily precipitation time series for the study region (box in Figure 1) for August and September (hereafter referred to as AS) in each year. We focus on rainfall amounts for these 2 months because this is when the monsoon is typically at its peak and AEWs are most intense and frequent in the study region. We identify the day with the highest area-averaged rainfall amount for each year (day 0). We composite the 16 time series of precipitation centered on day 0 of each year and analyze the evolution of the environment in the study region (see Figure S2 in the supporting information). We conduct the same composite analysis for the top 2, top 5, and top 10 heaviest rainfall days of each year and found that the peak in rainfall and corresponding changes in atmospheric conditions are consistent (see Figures S3 and S4 in the supporting information). We discuss the results from the top 5 rainy day composites—a total of 80 cases composited (Figures 1g–1j).

5.1. Composites of Area-Averaged Terms

To understand how the atmospheric conditions change along with the precipitation time series, we create composites for the midlevel (700–500 hPa) meridional wind component, moisture convergence, and rain type centered on the maximum rainfall day (Figures 1g–1j). The method for calculating moisture convergence is described in Text S1 in the supporting information. The average peak daily rainfall measures at about 26 mm day^{-1} during AS for the study region, significantly (at the 1% level using a one-sided t test assuming unequal sample variances) higher than the 8–13 mm day^{-1} recorded in 5 days before and after this peak (Figure 1g).

We extract the rain type from the TRMM PR data and calculate rain type fractions. We find the fraction of the total rainfall that is contributed by convective (ConvRain) or stratiform (StratRain) rain, and the fraction of region is experiencing either convective (AreaConv) or stratiform (AreaStrat) rain. The rain type fractions show that convective rain contributes more than 50% to the total rainfall in a small fraction (8–9%) of our study area (Figure 1h). The simultaneous increases in the area experiencing stratiform rain and the amount of stratiform rain on day 0 suggest the presence of deep, mature convective system including an anvil cloud, such as a squall line (Figure 1h).

The midlevel meridional wind composite (Figure 1i) indicates that northerlies begin to intensify the day before the maximum rainfall day (day −1), while low-level (1000–850 hPa) moisture convergence and midlevel moisture divergence peak on the maximum rainfall day [Figure 1j, *Núñez Ocasio et al*. 2016]. Favorable conditions for MCSs (e.g., low-level convergence and midlevel divergence) exist ahead of the AEW trough. These composites suggest that AEWs are driving enhanced convective development through increasing low-level moisture convergence ahead of the trough leading to heavy precipitation events.

5.2. Composites of Reanalyses Atmospheric Variables

To further investigate the mechanisms for the offshore rainfall maximum, we analyze the evolution of the synoptic setup of the region from 5 days before to 5 days after the maximum rainfall day in AS (see Figures S5–S8 in the supporting information). We show a shortened version in Figure 2.

The AEJ shows up centered on 15°N in the midlevel composites (Figures 2a–2d). A band of moister air ($q = 5$ g kg^{-1}) at this level lies south of the AEJ, positioned over the ITCZ where maximum vertical transport of low-level moisture occurs in deep convection (Figures 2a, 2e, and 2i). Northeasterlies flow through our
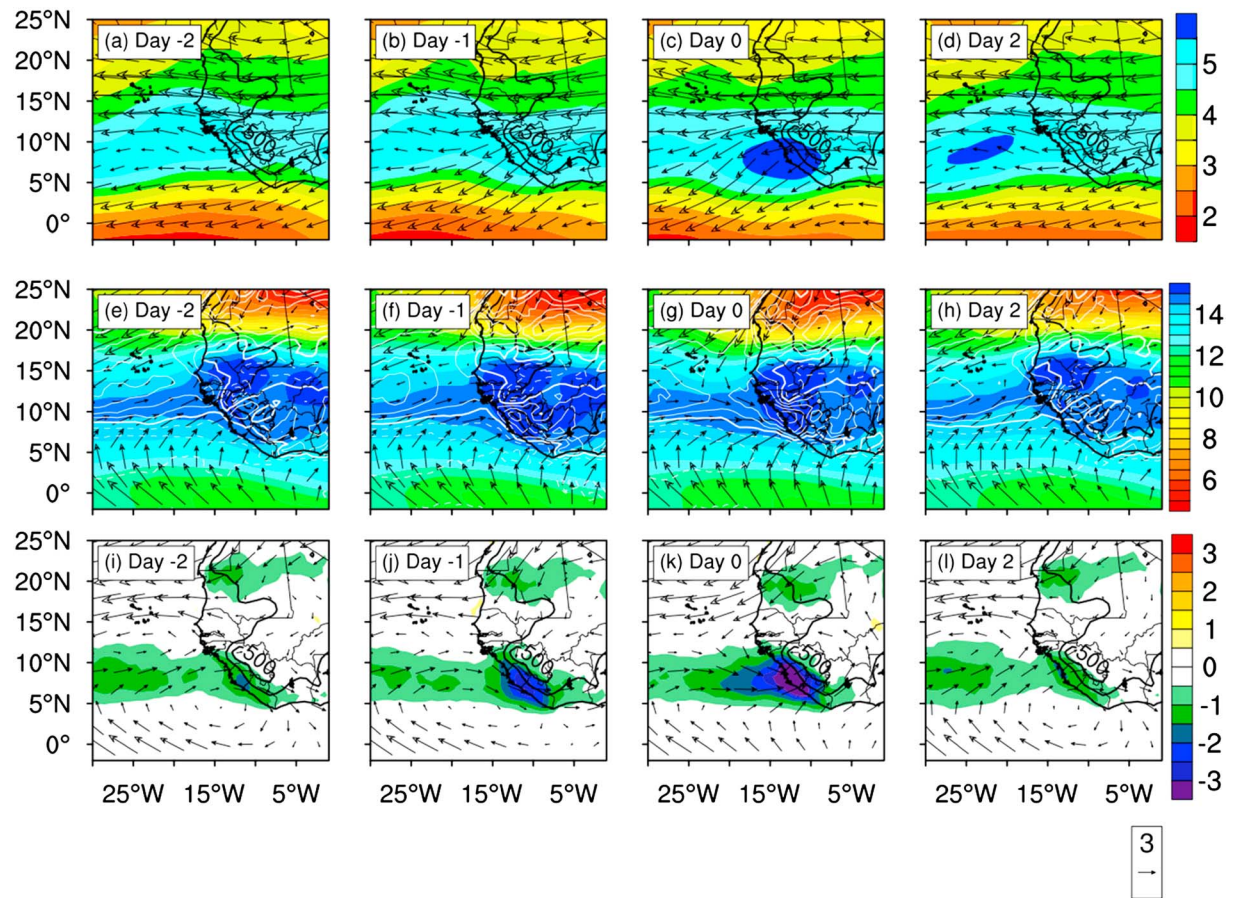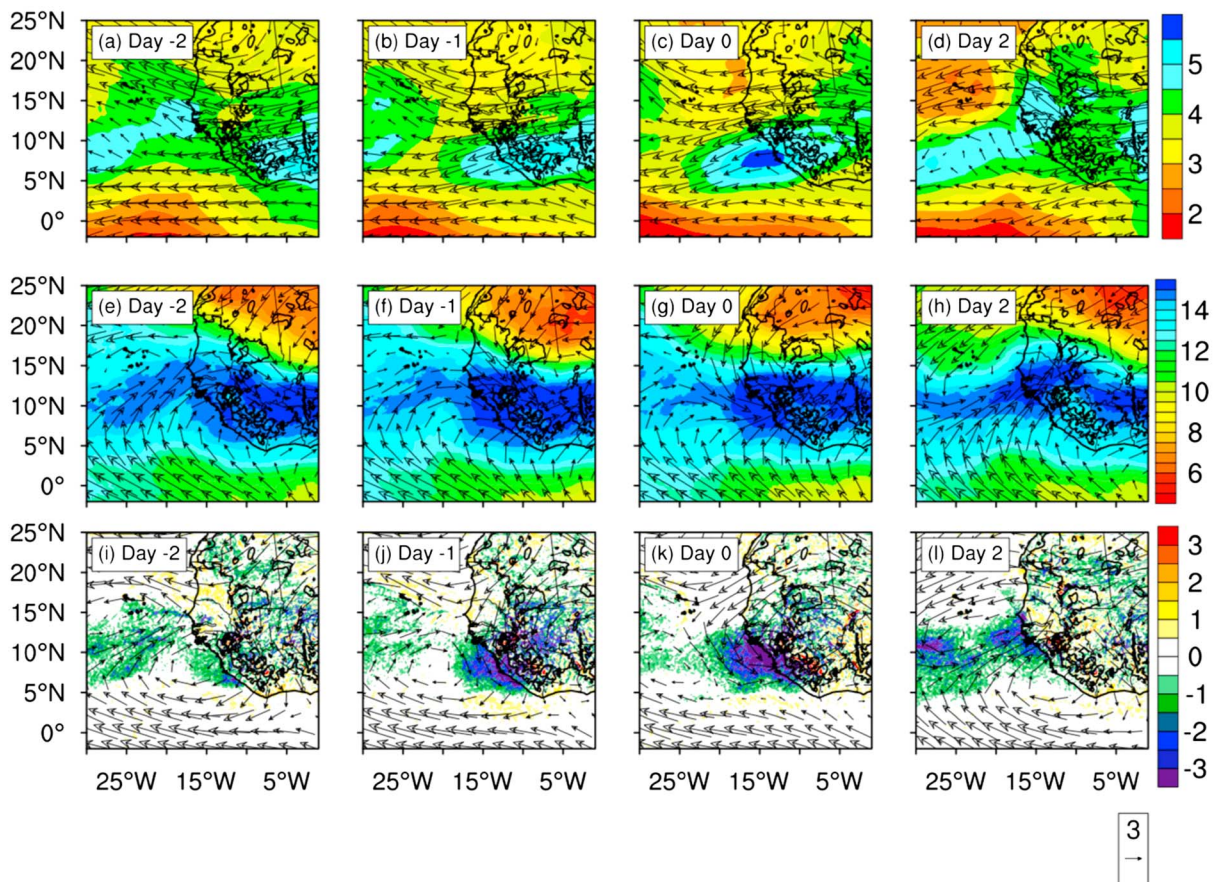
Figure 2. Composites of ERA-Interim (a–d) midlevel (700–500 hPa) *u-v* wind vectors (m s^{-1}) and *q* (g kg^{-1}, shaded); (e–h) low-level (1000–850 hPa) *u-v* wind vectors, *q* (g kg^{-1}, shaded), and relative vorticity (10^{-6} s^{-1}, white lines with intervals of 5 × 10^{-6} s^{-1}); and (i–l) 800 hPa *u-v* wind vectors and kinematic vertical moisture flux ($\omega \cdot q$) (g kg^{-1} Pa s^{-1}, shaded) from day −2 to day 2. The black contour lines over land show the topographic height in meters (250 m intervals). The reference vector is shown in the bottom right corner.

study region (20°–10°W, 5°–12°N) during days −5 to −4, becoming more zonal by day −3 (see Figures S5a–S5c in the supporting information). By day −2 the northeasterlies reappear between 0° and 10°W south of the AEJ (Figure 2a) and advance westward toward the coast (Figures 2b and 2c). On day 0, a local maximum in midlevel *q* appears in our study region indicating the moistening of the midlevels (Figure 2c). This *q* maximum is located over the offshore precipitation maximum (Figures 1a and 1b), which indicates the presence of deep convection. From days 1 to 2, the midlevel composites show that the moist air parcel embedded in the wave propagating off the coast and over the Atlantic (Figures 2c and 2d). After day 2, the midlevels slowly return to climatology with easterlies blowing through the region (see Figures S5i–S5k).

The low-level composites show onshore flow in our study region on all days (Figures 2e–2l); however, the moist onshore flow strengthens on day 0 (Figures 2f and 2k). The 850 hPa vortices north and south of the jet (centered at 20°N and 10°N, respectively) propagate across the region with the midlevel wave (Figures 2e and 2j). As these features reach the coast, the southern vortex enhances the low-level onshore flow (Figures 2f and 2k). Kinematic vertical moisture flux also increases at the coast as the strong low-level onshore flow interacts with the topography and enhanced low-level convergence and cyclonic vorticity ahead of the wave trough drive ascent (Figures 2f and 2k). On day 1 the low-level vortex (centered at 12.5°N) moves offshore with the midlevel wave (see Figure S7g). Despite the passage of the wave and its vortex, the low-level onshore flow remains strong in the study region on day 1; however, the vertical moisture flux weakens at the coast suggesting the significance of the wave's influence in driving the convection in heavy precipitation events. Also, while the wave enhances the convective development at the coast, the latent heat release from convection provides a major source of wave energy that leads to extra development

Figure 3. Composites of WRF TOPO (a–d) midlevel (700–500 hPa) u-v wind vectors (m s^{-1}) and q (g kg^{-1}, shaded), (e–h) low-level (1000–850 hPa) u-v wind vectors and q (g kg^{-1}, shaded), and (i–l) 800 hPa u-v wind vectors and $\omega \cdot q$ (g kg^{-1} Pa s^{-1}, shaded) from day −2 to day 2. The black contour lines over land show the topographic height in meters (250 m intervals). The reference vector is shown in the bottom right corner.

in AEWs [e.g., *Holton*, 1972; *Nitta*, 1972]. Enhanced AEW development can also be attributed to the topographically generated cyclogenic region in the lee of the mountains (with respect to the motion of the waves) [*Zehnder*, 1991; *Zehnder et al.*, 1999].

We measure the terrain's influence on the low-level flow using the upslope (northeastward) wind (see Figures S8 and S9). Before day 0 the winds in the upslope direction have two offshore maxima located west (6°–10°N, 10°–20°W) and south (2°–6°N, 2°–6°W) of the Guinea Highlands (see Figures S8a–S8b). On the maximum rainfall day, the maximum located west of the terrain shifts south to where the stronger onshore flow is at an angle to the coastline (see Figure S8c). On day 0 the maximum winds in the upslope direction is collocated with the maxima in the vertical moisture flux, midlevel moisture, and precipitation (Figures 2c, 2k, and S8c).

5.3. Composites of Atmospheric Variables in WRF Sensitivity Studies

To explore the relevance of topographic enhancement of AEWs to the West African offshore rainfall maximum, we return to the WRF sensitivity simulations introduced in section 4. Due to the smaller dataset, maximum rainfall days for the WRF simulations are defined as days experiencing at least 25% more rainfall than the mean daily rainfall in the study region (see Figure S10) and composites are conducted between 3 days before and after the maximum rainfall day. Composites are based on 9, 11, and 10 maximum rainfall days in TOPO, HALF, and FLAT, respectively. The observations and model composite analyses are not exact comparisons due to the difference in number of cases composited, but both composite analyses are representative of the rainiest days in the region (at least 25% more rainfall than the mean daily rainfall). Figures S11–S20 in the supporting information show the full composites, and we show shortened versions here in Figures 3 and 4.
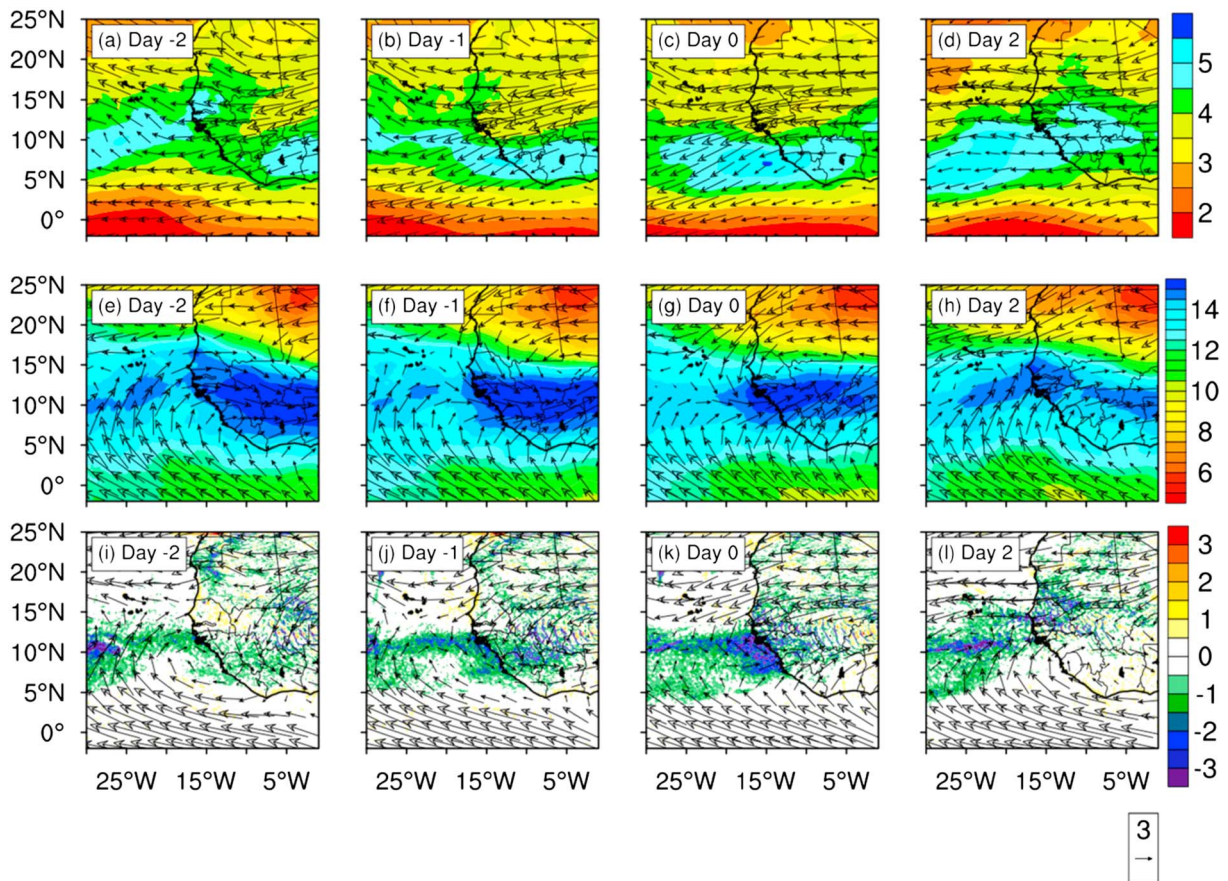
Figure 4. Same as Figure 3 but for FLAT simulation.

Similarly to the reanalyses, in TOPO a band of moister air ($q = 4$–$5\,g\,kg^{-1}$) is located south of the AEJ and above the ITCZ (Figures 3a and 3e). However, there is more curvature in the jet and preday 0, a midlevel ridge is propagating toward the coast, and its associated 850 hPa anticyclone is located in the study region (Figures 3a and 3i). As the midlevel ridge propagates away from the coast, the presence of a midlevel trough and its associated 850 hPa cyclone enhances the low-level onshore flow, and vertical moisture flux strengthens (Figures 3b, 3c, 3f, 3g, 3j, and 3k). The maximum in midlevel q is collocated with the maximum vertical moisture flux (Figures 3c and 3k) over the modeled offshore precipitation maximum (Figure 1d), indicating deep convection. After day 0, the convection and the wave propagate away from the coast into the Atlantic similar to the reanalyses composites (Figures 3d and 2d). The finer resolution of the WRF model captures the enhanced vertical moisture flux over the terrain better than the reanalyses (Figures 3j and 3k and 2j and 2k), coinciding with the strong upslope wind. However, the maximum in the moisture flux is always near the coast near the offshore maximum in upslope wind suggesting the importance of frictional uplift at the coastline.

The composites for HALF display similar patterns to both TOPO and the ERA composites but with a notably weaker midlevel wave (see Figure S14). Weaker onslope winds and vertical moisture flux lead to less convective development at the coast (see Figures S14k-S14o and S17). This weakening trend continues in FLAT; a weak midlevel wave propagates through the study region, but very little convective development is observed at the coast (Figures 4a–4d). There is still strong low-level onshore flow (Figures 4e–4h), and therefore strong moisture advection that is further enhanced on day 0 by the low-level cyclonic vorticity associated with the wave (Figures 4g and 4k). The absence of the topography allows the onshore monsoon flow to advance further inland, and the upslope wind is strong both over land and offshore. However, maximum ascent is offshore, and there is very little indication of rising air over land at low levels (Figures 4i–4l). This result indicates the role of the coastal topography in forcing ascent and creating favorable conditions for

mesoscale cyclogenesis onshore. This result is related to findings in *Martin and Thorncroft* [2015] where the degraded simulation of AEWs propagating off the West African coast in phase 5 of the Coupled Model Intercomparison Project models is related to the resolution of the Guinea Highlands. The representation of topography is important for the simulation of convection over the Guinea Highlands and the reinvigoration of AEWs as they propagate into the Atlantic [*Daloz et al.*, 2012; *Martin and Thorncroft*, 2015].

6. Conclusions

Analyses of 16 years of 3-hourly rainfall data indicate that the persistent rainfall maximum offshore of West Africa is closely related to AEWs and the enhancement of the low-level upslope flows near the Guinea Highlands. Composites of observed daily rainfall and meridional winds centered on the maximum rainfall days showed strong northerly winds, which supports the link between increased rainfall in the study region and the low-level convergence zone ahead of an AEW (the northerly phase of the wave). Rain type composites showed that convective rain dominates throughout the region, while stratiform rain increases in intensity indicating the presence of a deep mature convective system. Map composites of atmospheric variables from ERA-Interim reanalyses and the WRF simulations also support the connection between peak rainfall events and AEW activity in the study region. The AEW and its associated low-level cyclonic vortex enhance low-level convergence and forced uplift due to both frictional convergence at the coastline and interaction with topography creating suitably environmental conditions necessary for the development of intense precipitating events.

The amplitude of the rainfall maximum is reduced as topography is diminished (HALF and FLAT simulations). The elimination of the Guinea Highlands (FLAT) results in the absence of forced ascent in the coastal zone adjacent to the rainfall maximum, whereas the Highlands (TOPO and HALF) enhance convection near the coast. AEWs are often observed to experience extradevelopment over the Guinea Highlands. Consistent with this result, weaker AEJ and AEWs are diagnosed in the FLAT sensitivity model run compared to the more realistic TOPO run, thereby reducing the likelihood of both enhanced convective development of these weaker AEW-MCS systems and cyclogenesis at the coast. Our results provide evidence of the mechanism that enhanced topography at the coast-continent interface influences AEW and convective storm development. Understanding of the mechanisms leading to convective storm development and the offshore rainfall maximum can guide configuration of models to improve forecasts of the AEW-MCS systems that can become tropical cyclone precursor disturbances.

References

Chen, F., and J. Dudhia (2001), Coupling an advanced land surface-hydrology model with the Penn State-NCAR MM5 modeling system. Part I: Model implementation and sensitivity, *Mon. Weather Rev.*, *129*, 569–585.

Daloz, A. S., F. Chauvin, K. Walsh, S. Lavender, D. Abbs, and F. Roux (2012), The ability of general circulation models to simulate tropical cyclones and their precursors over the North Atlantic main development region, *Clim. Dyn.*, *39*, 1559–1576, doi:10.1007/s00382-012-1290-7.

Dee, D. P., et al. (2011), The ERA-Interim reanalysis: Configuration and performance of the data assimilation system, *Q. J. R. Meteorol. Soc.*, *137*, 553–597.

DeLonge, M. S., J. D. Fuentes, S. Chan, P. A. Kucera, E. Joseph, A. T. Gaye, and B. Daouda (2010), Attributes of mesoscale convective systems at the land-ocean transition in Senegal during NASA African Monsoon Multidisciplinary Analyses 2006, *J. Geophys. Res.*, *115*, D10213, doi:10.1029/2009JD012518.

Dudhia, J. (1989), Numerical study of convection observed during the winter monsoon experiment using a mesoscale two-dimensional model, *J. Atmos. Sci.*, *46*, 3077–3107.

Fuentes, J. D., B. Geerts, T. Dejene, P. D'Odorico, and E. Joseph (2008), Vertical attributes of precipitation systems in West Africa and adjacent Atlantic Ocean, *Theor. Appl. Climatol.*, *92*, 181–193.

Grell, G. A., and S. R. Freitas (2013), A scale and aerosol aware stochastic convective parameterization for weather and air quality modeling, *Atmos. Chem. Phys. Discuss.*, *13*, 23,845–23,893.

Guy, N., and S. A. Rutledge (2012), Regional comparison of West African convective characteristics: A TRMM-based climatology, *Q. J. R. Meteorol. Soc.*, *138*, 1179–1195.

Guy, N., S. A. Rutledge, and R. Cifelli (2011), Radar characteristics of continental, coastal, and maritime convection observed during AMMA/NAMMA, *Q. J. R. Meteorol. Soc.*, *137*, 1241–1256.

Hamilton, H. L. (2016), Relationships between rainfall characteristics and environmental predictors in the West African Region, Doctoral dissertation, The Pennsylvania State Univ., University Park, Pa. [Available at https://etda.libraries.psu.edu/catalog/8s45q876k.]

Holton, J. R. (1972), *An Introduction to Dynamic Meteorology*, pp. 373–376, Academic Press, New York.

Hong, S. Y., and J. O. Lim (2006), The WRF single-moment 6-class microphysics scheme (WSM6), *J. Korean Meteorol. Soc.*, *42*, 129–151.

Hong, S. Y., Y. Noh, and J. Dudhia (2006), A new vertical diffusion package with explicit treatment of entrainment processes, *Mon. Weather Rev.*, *134*, 2318–2341.

Huffman, G. J., D. T. Bolvin, E. J. Nelkin, D. B. Wolf, R. F. Alder, G. Gu, Y. Hong, K. P. Bowman, and E. F. Stocker (2007), The TRMM multisatellite precipitation analysis (TMPA): Quasi-global, multiyear, combined-sensor precipitation estimates at fine scales, *J. Hydrometeorol.*, *8*, 38–55.

Jenkins, G., et al. (2010), Coastal observations of weather features in Senegal during the African monsoon multidisciplinary analysis special observing period 3, *J. Geophys. Res.*, *115*, D18108, doi:10.1029/2009JD013022.

Jiménez, P. A., J. Dudhia, J. F. Gonález-Rouco, J. Navarro, J. P. Montávez, and E. García-Bustamente (2012), A revised scheme for the WRF surface layer formulation, *Mon. Weather Rev.*, *140*, 898–918.

Kiladis, G. N., C. D. Thorncroft, and N. G. Hall (2006), Three dimensional structure and dynamics of the African easterly waves. Part II: Observations, *J. Atmos. Sci.*, *63*, 2212–2230.

Kummerow, C., W. Barnes, T. Kozu, J. Shiue, and J. Simpson (1998), The tropical rainfall measuring mission TRMM sensor package, *J. Atmos. Oceanic Technol.*, *15*, 809–817.

Laing, A. G., and J. M. Fritsch (1993), Mesoscale convective complexes in Africa, *Mon. Weather Rev.*, *121*, 2254–2263.

Martin, E. R., and C. Thorncroft (2015), Representation of African Easterly Waves in CMIP5 models, *J. Clim.*, *28*, 7702–7715, doi:10.1175/JCLI-D-15-0145.1.

Mathon, V., H. Laurent, and T. Lebel (2002), Mesoscale convective system rainfall in the Sahel, *J. Appl. Meteorol. Climatol.*, *41*, 1081–1092.

Mlawer, E. J., S. J. Taubman, P. D. Brown, M. J. Iacono, and S. A. Clough (1997), Radiative transfer for inhomogeneous atmosphere: RRTM, a validated correlated-k model for the long wave, *J. Geophys. Res.*, *102*, 16,663–16,682, doi:10.1029/97JD00237.

Mozer, J. B., and J. A. Zehnder (1996a), Lee vorticity production by large-scale tropical mountain ranges. Part I: Eastern North Pacific tropical cyclogenesis, *J. Atmos. Sci.*, *53*, 521–538.

Mozer, J. B., and J. A. Zehnder (1996b), Lee vorticity production by large-scale tropical mountain ranges. Part II: A mechanism for the production of African waves, *J. Atmos. Sci.*, *53*, 539–549.

Nicholls, S. D., and K. I. Mohr (2010), An analysis of the environments of intense convective systems in West Africa in 2003, *Mon. Weather Rev.*, *138*, 3721–3739.

Nitta, T. S. (1972), Energy budget of wave disturbances over the Marshall Islands during the years of 1956 and 1958, *J. Meteorol. Soc. Jpn.*, *50*, 71–84.

Núñez Ocasio, K. M., H. L. Hamilton, J. L. Evans, and J. D. Fuentes (2016), A 16-year climatology of the West African offshore rainfall maximum, Poster S48. *96th AMS Annual Meeting*. 10-14 January 2016, New Orleans, La. [Available at https://ams.confex.com/ams/96Annual/webprogram/15STUDENT.html]

Skamarock, W. C., J. B. Klemp, J. Dudhia, D. O. Gill, D. M. Barker, M. G. Duda, X.-Y. Huang, W. Wang, and J. G. Powers (2008), A description of the advanced research WRF version 3, NCAR Tech. Note NCAR/TN-475+STR, 113 pp. doi:10.5065/D68S4MVH.

Thorncroft, C. D., and K. Hodges (2001), African easterly wave variability and its relationship to Atlantic tropical cyclone activity, *J. Clim.*, *14*, 1166–1179.

Varble, A., E. J. Zipser, A. M. Fridlind, P. Zhu, A. S. Ackerman, J.-P. Chaboureau, S. Collis, J. Fan, A. Hill, and B. Shipway (2014a), Evaluation of cloud-resolving and limited area model intercomparison simulations using TWP-ICE observations: 1. Deep convective updraft properties, *J. Geophys. Res. Atmos.*, *119*, 13,891–13,918, doi:10.1002/2013JD021371.

Varble, A., E. J. Zipser, A. M. Fridlind, P. Zhu, A. S. Ackerman, J.-P. Chaboureau, J. Fan, A. Hill, B. Shipway, and C. Williams (2014b), Evaluation of cloud-resolving and limited area model intercomparison simulations using TWP-ICE observations: 2. Precipitation microphysics, *J. Geophys. Res. Atmos.*, *119*, 13,919–13,945, doi:10.1002/2013JD021372.

World Meteorological Organization (2014), [Available at https://www.wmo.int/pages/prog/www/IMOP/publications/CIMO-Guide/Prelim-2014Ed/Prelim2014Ed_PI_Ch-6.pdf.]

Xu, W., and E. J. Zipser (2012), Properties of deep convection in tropical continental, monsoon, and oceanic rainfall regimes, *Geophys. Res. Lett.*, *39*, L07802, doi:10.1029/2012GL051242.

Zehnder, J. A. (1991), The interaction of planetary-scale tropical easterly waves with topography: A mechanism for the initiation of tropical cyclones, *J. Atmos. Sci.*, *127*, 1217–1230.

Zehnder, J. A., and R. L. Gall (1991), On a mechanism for orographic triggering of tropical cyclones in the Eastern North Pacific, *Tellus*, *43*, 25–36.

Zehnder, J. A., D. M. Powell, and D. L. Ropp (1999), The interaction of easterly waves, orography, and the intertropical convergence zone in the genesis of Eastern Pacific tropical cyclones, *Mon. Weather Rev.*, *127*, 1566–1585.

Zipser, E. J. (1994), Deep cumulonimbus cloud systems in the tropics with and without lightning, *Mon. Weather Rev.*, *122*, 1837–1851.